A structural homologue of the plant receptor D14 mediates responses to strigolactones in the fungal phytopathogen Cryphonectria parasitica

Valentina Fiorilli, Marco Forgia, Alexandre de Saint Germain, Giulia D ' Arrigo, David Cornu, Philippe Le Bris, Salim Al-Babili, Francesca Cardinale, Cristina Prandi, Francesca Spyrakis, et al.

▶ **To cite this version:**

Valentina Fiorilli, Marco Forgia, Alexandre de Saint Germain, Giulia D ' Arrigo, David Cornu, et al.. A structural homologue of the plant receptor D14 mediates responses to strigolactones in the fungal phytopathogen Cryphonectria parasitica. New Phytologist, In press, 234, pp.1003-1017. 10.1111/nph.18013 . hal-03558570

HAL Id: hal-03558570
https://hal.science/hal-03558570

Submitted on 4 Feb 2022

HAL is a multi-disciplinary open access archive for the deposit and dissemination of scientific research documents, whether they are published or not. The documents may come from teaching and research institutions in France or abroad, or from public or private research centers.

L'archive ouverte pluridisciplinaire **HAL**, est destinée au dépôt et à la diffusion de documents scientifiques de niveau recherche, publiés ou non, émanant des établissements d'enseignement et de recherche français ou étrangers, des laboratoires publics ou privés.

Distributed under a Creative Commons Attribution 4.0 International License

Check for updates

DR ALEXANDRE DE SAINT GERMAIN (Orcid ID : 0000-0003-2814-7234)
DR SALIM AL-BABILI (Orcid ID : 0000-0003-4823-2882)
DR FRANÇOIS-DIDIER BOYER (Orcid ID : 0000-0001-9855-7234)
PROF. LUISA LANFRANCO (Orcid ID : 0000-0002-3961-2552)

Article type : Full paper

A structural homologue of the plant receptor D14 mediates responses to strigolactones in the fungal phytopathogen *Cryphonectria parasitica*

Valentina Fiorilli[1*], Marco Forgia[2*], Alexandre de Saint Germain[3*], Giulia D'Arrigo[4], David Cornu[5], Philippe Le Bris[3], Salim Al-Babili[6], Francesca Cardinale[7], Cristina Prandi[8], Francesca Spyrakis[4], François-Didier Boyer[9], Massimo Turina[2], Luisa Lanfranco[1]

[1]Università di Torino, Dipartimento di Scienze della Vita e Biologia dei Sistemi, Viale P.A. Mattioli 25, 10125, Torino, Italy

[2]Istituto per la Protezione Sostenibile delle Piante - CNR -, Strada delle Cacce 73, 10135, Torino, Italy

[3]Université Paris-Saclay, INRAE, AgroParisTech, Institut Jean-Pierre Bourgin (IJPB), Route de St. Cyr (RD10), 78026, Versailles, France

[4]Università di Torino, Dipartimento di Scienza e Tecnologia del Farmaco, via P. Giuria 11, 10125 Torino, Italy

[5]Université Paris-Saclay, CEA, CNRS, Institute for Integrative Biology of the Cell (I2BC), 1 Avenue de la Terrasse, 91198, Gif-sur-Yvette, France

[6]King Abdullah University of Science and Technology, Division of Biological and Environmental Science and Engineering, Thuwal 23955-6900, Saudi Arabia

[7]Università di Torino, Dipartimento di Scienze Agrarie, Forestali e Alimentari, Largo Braccini 2, 10095 Grugliasco, Italy

[8]Università di Torino, Dipartimento di Chimica, via P. Giuria 7, 10125, Torino, Italy

This article has been accepted for publication and undergone full peer review but has not been through the copyediting, typesetting, pagination and proofreading process, which may lead to differences between this version and the Version of Record. Please cite this article as doi: 10.1111/NPH.18013

This article is protected by copyright. All rights reserved

Accepted Article

[9]Université Paris-Saclay, CNRS, Institut de Chimie des Substances Naturelles, UPR 2301, 1 Avenue de la Terrasse, 91198, Gif-sur-Yvette, France

[*]These authors contributed equally to this work

Corresponding author:

Luisa Lanfranco

Department of Life Sciences and Systems Biology

University of Turin

Viale P.A. Mattioli 25, 10125, Torino, Italy

e-mail: luisa.lanfranco@unito.it telephone 00390116705969

Received: *22 December 2021*

Accepted: *26 January 2022*

ORCID:

Valentina Fiorilli	0000-0001-9805-1559
Marco Forgia	0000-0003-0101-1046
Alexandre de Saint Germain	0000-0003-2814-7234
David Cornu	0000-0003-0055-5666
Philippe Le Bris	0000-0002-3569-7595
Francesca Spyrakis	0000-0002-4016-227X
Giulia D'Arrigo	0000-0002-1113-2266
Francois Didier Boyer	0000-0001-9855-7234
Salim Al-Babili	0000-0003-4823-2882
Massimo Turina	0000-0002-9659-9470
Francesca Cardinale	0000-0001-9892-9325
Cristina Prandi	0000-0001-9510-8783
Luisa Lanfranco	0000-0002-3961-2552

This article is protected by copyright. All rights reserved

Accepted Article

Accepted Article

Summary

- Strigolactones (SLs) are plant hormones and important signaling molecules required to promote the arbuscular mycorrhizal (AM) symbiosis. While in plants an α/β-hydrolase, DWARF14 (D14), was shown to act as a receptor that binds and cleaves SLs, the fungal receptor for SLs is unknown.
- Since AM fungi are currently not genetically tractable, in this study, we used the fungal pathogen *Cryphonectria parasitica* for which gene deletion protocols exist, as a model, as we have previously shown that it responds to SLs. By means of computational, biochemical and genetic analyses we identified a D14 structural homologue, CpD14.
- Molecular homology modelling and docking support the prediction that CpD14 interacts with and hydrolyses SLs. The recombinant CpD14 protein shows α/β hydrolytic activity *in vitro* against the SLs synthetic analogue GR24; its enzymatic activity requires an intact Ser/His/Asp catalytic triad. CpD14 expression in the *d14-1* loss-of-function *Arabidopsis thaliana* line did not rescue the plant mutant phenotype. However, gene inactivation by knock-out homologous recombination reduced fungal sensitivity to SLs.
- These results indicate that CpD14 is involved in SLs responses in *C. parasitica* and strengthen the role of SLs as multifunctional molecules acting in plant microbe-interactions.

Key words

α/β-hydrolase, apocarotenoids, *Cryphonectria parasitica,* D14, fungus, perception, strigolactones

This article is protected by copyright. All rights reserved

Introduction

Cryphonectria parasitica is a bark pathogen which causes perennial necrotic lesions (cankers) on above-ground part of susceptible host trees. This fungus is still a major threat to American and European chestnut trees causing the blight disease, which leads to yield losses of fruit and wood (Rigling & Prospero, 2018).

C. parasitica is a model fungus for studying how mycovirus cause the hypovirulent phenotype, and a wealth of different approaches have only partially elucidated how severity of disease can be tempered by the presence of the *Cryphonectria hypovirus 1* (CHV1) (Eusebio-Cope et al., 2015). Notwithstanding the detailed account of virus-caused perturbation characterized with different approaches (Allen *et al.,* 2003; Choi and Nuss, 1992; Dawe *et al.,* 2009; Wang *et al.,* 2014), not much is known about the possible molecular signalling occurring between the plant and the fungus, resulting in pathogenicity (Lovat and Donnelly, 2019): no specific gene products, structural component or metabolite has been identified to play a role in the mutual recognition between plant and fungus, and novel molecules could be hypothesized among essential or accessory players.

A few years ago, we demonstrated that *C. parasitica* is sensitive to (±)-GR24, (GR24 hereafter) (Belmondo *et al.,* 2016), a synthetic analog of strigolactones, confirming what was also observed in several other plant pathogenic fungi (Dor *et al.,* 2011).

Strigolactones (SLs) are a class of carotenoid-derived phytohormones (Al-Babili & Bouwmeester 2015), characterized by a methylbutenolide moiety (D-ring) linked to a variable tricyclic lactone (ABC-ring system). SLs, which play a role in the regulation of several aspects of plant growth and development and responses to biotic and abiotic stress (Gomez-Roldan *et al.,* 2008; Umehara *et al.,* 2008; Lopez-Obando *et al.,* 2015; Ha et al. 2014; Waters *et al.,* 2017; Koltai & Prandi, 2019) were first described as plant metabolites able to stimulate seed germination in parasitic plants (Cook *et al.,* 1966). In addition, when released by roots in the soil, SLs also enhance the growth and metabolism of a group of beneficial symbiotic fungi (Akiyama *et al.,* 2005; Besserer et al., 2006; 2008; Salvioli *et al.,* 2016; Kamel *et al.,* 2017; Tsuzuki *et al.,* 2016; Genre *et al.,* 2013; Volpe *et al.,* 2020), favoring the establishment of the arbuscular mycorrhizal (AM) symbiosis a very ancient and widespread mutualistic association with plant roots (MacLean *et al.,* 2017; Lanfranco *et al.,* 2018a).

SLs seem therefore multifunctional molecules active on plants and microorganisms (Lopez-Raez *et al.,* 2017; Lanfranco *et al.,* 2018b; Rochange *et al.,* 2019; Schlemper *et al.,* 2017; Carvalhais *et*

This article is protected by copyright. All rights reserved

al., 2019).

To our knowledge, the mechanism of SLs perception in fungi is not known. On the contrary, SLs perception has been elucidated in plants (Waters *et al.,* 2017; Hamiaux *et al.,* 2012): the rice DWARF14 (D14) protein was described as a non-canonical receptor having the dual function of enzyme and receptor (Yao *et al.,* 2016; de Saint Germain *et al.,* 2016). D14 is an α/β-hydrolase that can bind and cleave SLs, by performing a nucleophilic attack on the D-ring. However, the hydrolytic event is currently debated as an essential process that promotes activation of D14 (Shabek *et al.,* 2018; Seto *et al.,* 2019; Bürger *et al.,* 2020). Upon SLs binding, D14 undergoes a conformational change to recruit downstream signaling components, such as the D3 protein, for triggering SLs responses (Yao *et al.,* 2018). A similar irreversible perception mechanism was proven for D14 homologues from other plant species including Arabidopsis (AtD14 Chevalier *et al.,* 2014, pea (RAMOSUS3 (RMS3) de Saint Germain 2016), petunia (DECREASED APICAL DOMINANCES (DAD2) Hamiaux *et al.,* 2012) and the root parasitic weed *Striga hermonthica* (ShHYPOSENSITIVE TO LIGHT7 (ShHTL7) Toh *et al.,* 2015; Yao *et al.,* 2017). A clear D14 homologue was not found in the genome of AM fungi (Tisserant *et al.,* 2013; Lin *et al.,* 2014), the most studied fungal system for SLs responses.

In this context, we decided to exploit the SLs-sensitive fungus *C. parasitica* for which, in contrast to AM fungi, stable genetic transformation protocols are available.

In this work, we tested the hypothesis that fungi possess D14 homolog proteins that could bind and hydrolyse SLs and that could eventually complement the mutation of the corresponding plant homologue. We identified a candidate D14 structural homologue in *C. parasitica* and called it CpD14 (CpD14); by means of molecular modeling analyses and biochemical characterization of the recombinant protein we demonstrated CpD14 binding and enzymatic activity on natural SLs and their synthetic analogues. The expression of *CpD14* in the *d14* loss of function *Arabidopsis thaliana* line did not rescue the plant mutant phenotype. However, gene inactivation by knock-out homologous recombination reduced *C. parasitica* sensitivity to SLs, indicating that the gene is indeed involved in SLs responses in this fungus.

Materials and Methods

Fungal strains. *C. parasitica* (Murrill) Barr. Δ*cpku80,* in this work considered a wild type (WT) strain, was chosen for its ability to generate double homologous recombination and enhance site directed mutagenesis efficiency (Lan *et al.,* 2008).

This article is protected by copyright. All rights reserved

Generation of *C. parasitica CpD14* mutant strains. *CpD14* knock-out strains (Δ*cpd14_48*, *Δcpd14_137*, Δ*cpd14_141)* were generated by site-directed double homologous recombination with a construct carrying a hygromycin B resistance cassette. The *CpD14* gene, including around 1 kb upstream and downstream sequences, was amplified using KOFor and KORev primers (Supporting Information Table S1). The 3477 bp long amplicon was cloned in pCR Zero blunt vector. The recombinant plasmid was digested with *Afe*I to delete a 293 bp portion in the gene sequence. The hygromycin B resistance cassette was amplified through PCR from the pCB1004 vector (Carroll *et al.,* 1994) using the Gibson assembly primer couple GibFor and GibRev (Supporting Information Table S1) and the PCR product was cloned in the digested plasmid through the Takara Infusion kit. The knock-out plasmid was linearized by restriction and transformed into protoplasts of the *C. parasitica* Δ*cpku80* strain. Hygromycin-resistant colonies were screened through PCR using primers amplifying full length *CpD14*. Transformed colonies where double homologous recombination had occurred gave a 2000 bp band instead of the normal PCR product of about 1000 bp. Selected mutants were grown on PDA media; conidia were harvested from one-month-old cultures and plated to obtain single-conidia colonies. A further PCR screening was carried out on single-conidia colonies from each independent mutant using primers as forward the KOFor primer and as reverse the hygromycin resistance cassette Hyg100For (Supporting Information Table S1), leading to a PCR product of about 1500 bp.

Fungal growth assays. *C. parasitica* strains were pre-cultivated for 3 days at 20°C on solid PDA medium. All standard cultivations were done under diurnal light conditions. Afterwards, one mycelial plug was transferred on solid B5 medium (Duchefa, 3.17 g/L) supplemented with 2% glucose as described in Fiorilli *et al.* (2021). The screening was carried out in 3.5 cm microtiter wells (7 mL medium/well). Stock solutions of (+)-2'-*epi* GR24; (–)-GR24; (+)-GR24; (–)-2'-*epi*-GR24 (MW 298.29) and of tolfenamic acid (an inhibitor of plant SLs receptors; Hamiaux *et al.,* 2018; MW 261.71) were prepared dissolving the powder in the appropriate solvent (acetone for GR24 stereoisomers and DMSO for tolfenamic acid) to obtain a 10 mM solution. The WT strain was analysed in triplicate on (+)-2'-*epi* GR24; (–)-GR24; (+)-GR24; (–)-2'-*epi*-GR24 (from 10^{-4} to 10^{-5} M) and acetone control in parallel. WT and Δ*cpd14* mutant strains were analysed in triplicate on (+)-GR24 (10^{-4} M), on tolfenamic acid (10^{-6} M), on both (+)-GR24 (10^{-4} M) and tolfenamic acid (10^{-6}M) and in parallel on acetone, DMSO, acetone + DMSO as corresponding control

This article is protected by copyright. All rights reserved

samples. Microtiter wells were kept in a dark room at 20°C and at 24, 48, 72 and 96 h the colony diameter of the hyphal radial growth was measured. No effect of the solvents was observed (data not shown). Pictures were taken at the edge of the colony, 96 h post-inoculation using a light microscope Primo Star Zeiss (Carl Zeiss MicroImaging, Göttingen, Germany) with a Leica DFC425 digital camera attached (Leica Microsystems, Wetzlar, Germany) to highlight possible alterations in hyphal growth and morphology.

Molecular homology modelling and docking. The CpD14 sequence was used as query to perform a template search in the Protein Data Bank (PDB) database with the PSI-BLAST algorithm. The DAD2 X-ray structure (PDB code: 4dnp) was identified as the best possible template, according to the sequence identity and coverage, and used to build the CpD14 three-dimensional model with the SWISS-MODEL server (Waterhouse *et al.,* 2018). The quality assessment of the predicted model was validated by building the Ramachandran plot using the RAMPAGE server (http://mordred.bioc.cam.ac.uk/~rapper/rampage.php).

Docking simulations with natural and synthetic analogues of SLs were performed using the GOLD suite version 5.5, as done previously (Lombardi et al. 2017 Sanchez et al. 2018). The pocket of interest was defined to contain all the residues within 10 Å from a reference atom (CD2, Leu188). Due to some protruding residues in the ligand-binding pocket, and to ensure a correct positioning of the compounds into the pocket, side chain flexibility was allowed to the bulkiest residues (Tyr164, Glu227, Met253). Moreover, to reproduce the catalytic environment, Ser104 and His181 were simulated respectively in the deprotonated and protonated state. (+)-GR24, (–)-2'-*epi*-GR24 and (+)-strigol were submitted to 15 genetic algorithm runs and the CHEMPLP score function was used to select the best pose.

Molecular dynamics simulation of the CpD14 model was performed using the GROMACS version 4.6.1 (Pronk *et al.,* 2013). Protein topology was generated with the Amber99SBILDN force field (Hornak, *et al.,* 2006) and the protein was solvated using the TIP3P water molecules (Jorgensen *et al.,* 1983) in a 12 Å cubic box. The box and the MD set-up were built using the BiKi Life Sciences suite (Decherchi *et al.,* 2018; Spyrakis *et al.,* 2015). The system was subjected to 5000 steps of energy minimization with the steepest-descent algorithm. Then, four equilibration steps were carried out: 500 ps in the NVT ensemble at 100 K, 200 K and 300 K, and 1 ns in the NPT ensemble with an integration step of 2 fs. Finally, the system was simulated for 200 ns in the NVT ensemble.

This article is protected by copyright. All rights reserved

Cloning, expression and purification of recombinant proteins. The *CpD14* full-length cDNA was amplified from the RNA of *C. parasitica* grown in liquid cultures using a forward primer (CpD14-F) containing a *Bgl*II site and a reverse primer (CpD14-R) containing an *Kpn*I site (Supporting Information Table S1); the sequence was cloned into the pHUE vector. To obtain the mutated version of the protein, the vector pHUE containing the complete coding sequence of CpD14 was amplified through PCR using a forward primer carrying two mutated nucleotides. The forward primer (CpD14For) was used with the reverse primer 309Rev (Supporting Information Table S1) to amplify a linearized full-length plasmid carrying the mutation in position 309 and 310 to change the codon usage from Ser to Ala. The obtained linearized plasmid was phosphorylated and ligated with a T4 ligase (Thermo Fisher Scientific). The $CpD14^{S104A}$ specific mutation was confirmed through sequencing.

For CpD14 protein expression, the full-length coding sequences from *C. parasitica* were amplified by PCR using the recombinant plasmid pHUE-*CpD14* as template and specific primers (CpD14_attb1_HRV3C and CpD14_attb2 (Supporting Information Table S1) containing a protease cleavage site for tag removal, and subsequently cloned into the pGEXT-4T-3 expression vector.

Preparation of GR24 isomers and GC probes. (+)-GR24, (-)-GR24, (+)-2'-*epi*-GR24, (-)-2'-*epi*-GR24 were separated from (±)-2'-*epi*-GR24 and (±)-GR24 by chiral supercritical fluid chromatography as described in de Saint Germain *et al.,* (2016, 2019). Probes (GC486, GC240, GC242) were prepared also according to de Saint Germain *et al.* (2016).

Enzymatic degradation of GR24 isomers by purified proteins. The ligand (10 µM) was incubated without and with purified proteins (5 µM) for 150 min at 25ºC in 0.1 mL phosphate buffer saline (PBS - 100 mM phosphate, pH 6.8, 150 mM NaCl) in presence of (±)-1-indanol (100 µM) as internal standard. The solutions were acidified to pH 1 by addition of trifluoroacetic acid (2 µL) to quench the reaction and centrifugated (12 min, 12,000 tr/min). The samples were subjected to RP-UPLC-MS analyses using a UPLC system equipped with a PDA and a Triple Quadrupole mass spectrometer Detector (Acquity UPLC-TQD, Waters, USA). RP-UPLC (HSS C_{18} column, 1.8 µm, 2.1 mm × 50 mm) with 0.1% formic acid in CH_3CN and 0.1% formic acid in water (aq. FA, 0.1%, v/v, pH 2.8) as eluents [10% CH_3CN, followed by linear gradient from 10 to

This article is protected by copyright. All rights reserved

100% of CH_3CN (4 min)] at a flow rate of 0.6 mL/min. The detection was performed by PDA and using the TQD mass spectrometer operated in electrospray ionization positive mode at 3.2 kV capillary voltage. The cone voltage and collision energy were optimized to maximize the signal and was respectively 20 V for cone voltage and 12 eV for collision energy and the collision gas was argon at a pressure maintained near of $4.5.10^{-3}$ mBar.

Enzymatic assay with pro-fluorescent probes

These assays were performed as described in de Saint Germain *et al.* (2016), using a TriStar LB 941 Multimode Microplate Reader (Berthold Technologies).

Temperature melts proteins *nanoDSF*. Proteins were diluted in PBS to ~10 µM concentration. Ligand was tested at the concentration of 200 µM. The intrinsic fluorescence signal was measured as a function of increasing temperature in Prometheus NT.48 fluorimeter (Nanotemper™), with 55% excitation light intensity and 1°C/minute temperature ramp. Analyses were performed on capillaries filled with 10 µL of respective samples. Intrinsic fluorescence signal expressed by the 350 nm/330 nm emission ratio, which increases as the proteins unfold, is plotted as a function of temperature. The plots are one of the three independent data collections that were performed for each protein.

Intrinsic tryptophan fluorescence assays and determination of the dissociation constant K_D. These assays have been performed as described in de Saint Germain *et al.* (2016), using Spark® Multimode Microplate Reader from Tecan.

Direct ESI-MS in denaturant conditions. Mass spectrometry measurements were performed with an electrospray Q-TOF mass spectrometer (Waters) equipped with the Nanomate device (Advion, Inc.). The HD_A_384 chip (5 µm I.D. nozzle chip, flow rate range 100-500 nL/min) was calibrated before use. For ESI−MS measurements, the Q-TOF instrument was operated in RF quadrupole mode with the TOF data being collected between *m/z* 400−2990. Collision energy was set to 10 eV and argon was used as collision gas. Mass spectra acquisition was performed after denaturation of CpD14 ± ligand in 50% acetonitrile and 1% formic acid using Mass Lynx 4.1 (Waters) and Peakview 2.2 (Sciex). Deconvolution of multiply charged ions was performed by applying the MaxEnt algorithm (Sciex). The estimated mass accuracy is ± 2 Da. External

This article is protected by copyright. All rights reserved

calibration was performed with NaI clusters (2 µg/µL, isopropanol/H_2O 50/50, Waters) in the acquisition *m/z* mass range.

Localization of the fixation site of ligands on CpD14. RMS3-ligand, CpD14-ligand and $CpD14^{S104A}$-ligand mixtures were incubated for 10 min before to be submitted overnight to Glu-C proteolysis. Glu-C-generated peptides mixtures were analyzed by nanoLC-MS/MS with the Triple-TOF 4600 mass spectrometer (AB Sciex) coupled to the nanoRSLC ultra performance liquid chromatography (UPLC) system (Thermo Scientific) equipped with a trap column (Acclaim PepMap 100 C_{18}, 75 µm i.d. × 2 cm, 3 µm) and an analytical column (Acclaim PepMap RSLC C_{18}, 75 µm i.d.× 25 cm, 2 µm, 100 Å). Peptides were loaded at 5 µL/min with 0.05% TFA in 5% acetonitrile and peptides separation was performed at a flow rate of 300 $nl.min^{-1}$ with a 5 to 35% solvent B gradient in 40 min. Solvent A was 0.1% formic acid in water, and solvent B was 0.1% formic acid in 100% acetonitrile. NanoLC-MS/MS experiments were conducted in a Data Dependent acquisition method by selecting the 20 most intense precursors for CID fragmentation with Q1 quadrupole set at low resolution for better sensitivity. Raw data were processed with MS Data Converter tool (AB Sciex) and protein identification was performed using MASCOT (Matrix Science, London, UK) against the CpD14 sequence with oxidation of methionine and ligand-histidine adduct as variable modifications. Peptide and fragment tolerance were respectively set at 20 ppm and 0.05 Da. Only peptides with mascot ions score above identity threshold (25) calculated at 1% FDR.

Generation of *Arabidopsis thaliana* transgenic lines. The expression vectors for transgenic *Arabidopsis* were constructed by MultiSite Gateway Three-Fragment Vector Construction kit (Invitrogen) as described in de Saint Germain *et al.* (2016). The CpD14 CDS was tagged with 6xHA epitope tag at the C-terminus and under control of *AtD14* native promoter (0.8 kb). CpD14 CDS was PCR amplified from pGEX-4T-3-CpD14 plasmid and recombined into *pDONR221* (Invitrogen). The suitable combination of *AtD14* promoters, CpD14 CDS and 6xHA was cloned into the *pH7m34GW* final destination vectors by using three fragments recombination system (Karimi *et al.,* 2007), and named pD14::CpD14-6xHA. Transformation of *Arabidopsis Atd14-1* mutant (kindly provided by M. Waters, University of Western Australia, Australia) was performed

This article is protected by copyright. All rights reserved

according to the conventional dipping method (Clough & Bent, 1998), with *Agrobacterium* strain GV3101. Phenotypic analysis and protein extraction were performed on the T3 homozygous lines.

Plant phenotypic assays. Plants were grown in greenhouse. Experiments were carried out in summer, under long photoperiods (15-16 h per day); daily temperatures fluctuated between 18 °C and 25 °C. Peak levels of PAR were between 700 and 1000 μmol m^{-2} s^{-1}. Plants were watered twice a week with tap water. The number of rosette leaves was counted just after bolting of the main shoot, and the number of rosette branches longer than 5 mm was counted when the plants were 40 days old.

Expression profiles of *CpD14* and genes putatively involved in carotenoid biosynthesis and cleavage. To evaluate *CpD14* expression, WT and Δ*CpD14* mutant strains were grown in flasks containing B5 liquid media and kept in the dark on an orbital shaker for 96 h. After 96 h, liquid media supplemented with (+)-GR24 or (–)-2'-*epi*-GR24 (10^{-4}M) and acetone control in parallel were replaced in each flask, and after 48 h the mycelia were collected. To evaluate the expression of genes putatively involved in carotenoid biosynthesis and cleavage, WT was grown as described before for 7 days. Then, the liquid media supplemented with GR24 (10^{-4}M) or acetone were put in each flask, and after 48 h the mycelia were collected.

Total RNA was extracted using the Plant RNeasy Kit (Qiagen) and treated with TURBO™ DNase (Ambion) according to the manufacturer's instructions. cDNA synthesis was carried out on total RNA using Super-ScriptII (Invitrogen). RT-qPCR experiments were carried out using a Rotor Gene apparatus (Qiagen) as described in Volpe *et al.* (2020) with two technical replicates. The comparative threshold cycle method (Rasmussen, 2001) was used to calculate relative expression levels, with *C. parasitica CpGAPDH* and *CpTubulin* as reference genes. Oligonucleotide sequences are listed in Supporting Information Table S1.

Virulence assay. *CpD14* knockout mutant ability to induce canker on European chestnut (*Castanea sativa*) barks was assayed on dormant cuttings as previously described in Rostagno *et al.* (2010). Lesions were measured at 30 days post inoculation (dpi).

This article is protected by copyright. All rights reserved

Results

Characterization of CpD14

The sensitivity of *C. parasitica* to the four GR24 stereoisomers was evaluated using the *in vitro* growth assay previously described (Belmondo *et al.* 2016). At 10^{-4} M the stereoisomers whose stereochemistry corresponds to natural canonical SLs, (+)-GR24 (strigol-type) and (−)-2'-*epi*-GR24 (orobanchol-type) which have the D-ring with 2'*R* configuration, and the (−)- GR24 stereoisomer (2'*S* configuration), whose stereochemistry is not encountered in natural SLs, led to a reduction of fungal colony diameter at 72 and 96 h after inoculation (Supporting Information Fig. S1a). At 10^{-5} M only the two molecules corresponding to natural SL stereochemistry, (+)-GR24 and (−)-2'-*epi*-GR24, led to a transient decrease of radial growth (Supporting Information Fig. S1b). *C. parasitica* seems therefore more sensitive to GR24 stereoisomers whose stereochemistry corresponds to natural SLs.

To identify candidate D14 homologues in the genome of *C. parasitica* (Crouch *et al.,* 2020), a BlastP search, using the rice OsD14 sequence as query, was performed under low stringency conditions (Expected value 10). We identified a sequence of 302 amino acids, hereafter called CpD14, showing 26% identity with rice D14 and 25% with the petunia homologue DAD2, and 66% coverage. The putative catalytic triad, formed by serine, aspartate and histidine (Ser -S, Asp -D, His -H), and needed for SL hydrolysis (Hamiaux *et al.,* 2012), is conserved among the three sequences, as shown by the alignment (Fig. 1a; CpD14: Ser104, Asp251, His281; OsD14: Ser97, Asp218, His247; DAD2: Ser96, Asp217, His246).

In the absence of structural information, we built the 3D model of CpD14 by homology modelling. We first performed a similarity search within the PDB database using BLAST and identified the structure of DAD2 from petunia as the best possible template (PDB code 4dnp, Hamiaux *et al.,* 2012). DAD2 shares ~76% sequence identity with rice OsD14. The resulting protein model revealed the canonical α/β hydrolase fold and the lid of the binding site surrounded by four α helices (α1-α4 in Fig. 1b). The superposition with the DAD2 template showed completely overlapping catalytic residues (Fig. 1c), and a highly disordered loop next to helix α. The quality validation of the predicted model revealed that 87.9% of residues were in favored regions, 7.5% in allowed regions, and 4.6% in disallowed ones (Supporting Information Fig. S2). The model was also submitted to 200 ns-long molecular dynamics (MD) simulation, which further proved its stability, apart from the flexible close to helix α1.

Crystallographic evidence of the capability of SLs, in particular (+)-GR24, to bind OsD14 has

This article is protected by copyright. All rights reserved

been already reported (PDB code: 5dj5, Zhao *et al.,* 2015). Considering the high sequence identity shared by OsD14 with the DAD2 orthologue, the conservation of the general folding and of the critical residues (Supporting Information Fig. S3a), we hypothesized that SLs would be also able to bind DAD2, and the derived CpD14-like model. We, thus, performed molecular docking simulations of (+)-GR24, (–)-2'-*epi*-GR24 and (+)-strigol in the CpD14 model binding site (Fig. 1d; Supporting Information Fig. S3c, d). (+)-GR24 assumes a conformation similar to that in OsD14 (Supporting Information Fig. S3b). The D-ring faces the catalytic residues and H-bonds His281, the polar head of the ABC-ring system H-bonds to Tyr164 on α1, whereas the AB-ring system is partially exposed towards the solvent.

We next assessed the occurrence of CpD14 homologues in the fungal kingdom and attempted to trace their evolutionary history. We searched a number of representative fungal genomes of the Dikarya and Mucoromycota groups by BLASTp using CpD14 as query and retrieved the first hit. Furthermore, given that the *C. parasitica* genome contains a second protein with similarity to CpD14, we repeated a BLASTp search using, within each species, the first retrieved protein sequence as query. All these protein sequences were aligned by Clustal Omega and a phylogenetic tree was reconstructed through Maximum Likelihood method (Fig. 2). Notably, we could identify α/β hydrolase proteins showing the conserved SDH catalytic triad both in Dikarya and Mucoromycota. Nevertheless, homologues of this protein cannot be found in some fungal lineages such as the vast majority of Saccharomycotina and in some well-studied fungal model systems, i.e. *Neurospora crassa*, *Magnaporthe oryzae*, *Blumeria graminis*, and *Ustilago maydis*. In *Aspergillus flavus* the homologue is present, but it lacks the His residue in the catalytic domain. The closest homologues to CpD14 from each fungal genome (indicated in black in Fig. 2) cluster in three well supported clades, each only hosting proteins from Mucoromycota, Basidiomycota or Ascomycota. On the contrary, most of the proteins identified through the second BLASTp search in each specific genome sequence (in red in Fig. 2) are scattered in mixed branches with proteins from Basidiomycota. The only exceptions are proteins from *C. parasitica*, *Coniella lustricola* and *Oidiodendron maius,* which cluster only in the Ascomycota branch together with their first hit, showing evidence of possible more recent duplication events. In summary, our analysis shows a relatively widespread occurrence in fungal genomes of at least one putative homologue of CpD14 with a conserved catalytic domain (SDH catalytic triad). Phylogenetic reconstruction of these homologues shows some correlation with taxonomic groups. A second protein, sharing some similarity with fungal D14L-like proteins, is often present within single genomes, but with no

This article is protected by copyright. All rights reserved

clear association to taxonomically uniform groups.

As a further characterization of the *CpD14* gene, we searched for evidence of *CpD14* expression in the free-living mycelium and of possible regulation by 48-hour exposure to a GR24 racemic solution. *CpD14* was expressed in the fungus grown in liquid culture and no difference was observed upon GR24 treatment (Supporting Information Fig. S4a).

Taken as a whole these data indicate the occurrence of putative homologues of plant D14 in fungi.

CpD14 binds and hydrolyses SLs

We studied the putative interaction of the CpD14 protein with SLs by expressing and purifying the CpD14 protein *in vitro* and assessing its ability to interact with GR24 isomers (Fig. 3). The interaction between (+)-GR24 and CpD14 was confirmed using tryptophan intrinsic fluorescence assay (Fig. 3 a,b; Supporting Information Fig. S5), even if a lower affinity was observed in comparison with RMS3/PsD14 (K_D = 202.70 ± 41.12 µM *versus* 9.33 ± 4.27 µM), the SL receptor described in pea (de Saint Germain *et al.,* 2016). To confirm this interaction, we used nano-differential scanning fluorimetry (nanoDSF) recording changes in tryptophan fluorescence (ratio 350 nm/330 nm) during protein denaturation. We highlighted interactions by noticing a change of initial fluorescence ratio, but we failed to determine the CpD14 melting temperature due to the intrinsic nature of the protein. Therefore, this technique did not allow us to determine potential CpD14 conformational changes as it was done with RMS3, where (+)-GR24 (strigol-type) and (–)-2'-*epi*-GR24 (orobanchol-type) induce a larger destabilization in comparison with (–)-GR24 and (+)-2'-*epi*-GR24, whose stereochemistry is not encountered in natural SLs. We detected no change in the CpD14 melting temperature (Supporting Information Fig. S5) with the four GR24 isomers.

As a further step, by using the internal standard (±)-1-indanol the cleavage activity of the CpD14 towards (+)-GR24, (–)-GR24, (+)-2'-*epi*-GR24 and (–)-2'-*epi*-GR24 was quantified and compared to the cleavage activity of RMS3 and CpD14^{S104A}, a CpD14 sequence variant where the serine at position 104 of the putative SDH catalytic triad was replaced with an alanine. CpD14 efficiently cleaved (+)-GR24 and (–)-2'-*epi*-GR24, like RMS3, but poorly (–)-GR24 and (+)-2'-*epi*-GR24 (Fig. 3c). No significant cleavage activity was recorded for CpD14^{S104A} with any of the GR24 isomers tested (Fig. 3c). These data highlight that CpD14 hydrolyses GR24 isomers with the configuration of natural SLs and that this hydrolysis cannot occur without an intact catalytic triad. GC profluorescent probes, which were used to determine RMS3 kinetics (de Saint Germain *et al.,*

This article is protected by copyright. All rights reserved

2016; de Saint Germain *et al.,* 2021), were poorly hydrolysed by CpD14 (Supporting Information Fig. S6). However, after incubating (+)-GR24 and (−)-GR24 with CpD14 and recording mass spectrometry spectra in denaturing conditions, we detected in all cases a mass shift corresponding to the formation of a covalent complex, with the D-ring (Fig. 3d,e,f,g,h,i). According to the hydrolysis results (Fig. 3c), the formation of the covalent complex was favoured with (+)-GR24 (Fig. 3e) in comparison with (−)-GR24 (Fig. 3f), while no complex was observed for CpD14^{S104A} (Fig. 3g). Fragmentation spectra of unmodified and ligand-modified peptides unambiguously supported the D-ring being specifically attached to His281 of the catalytic triad (Fig. 3h,i). We therefore demonstrated that CpD14 forms a stable intermediate with the D-ring, as previously reported for other SL receptors (PsD14/RMS3, AtD14, D14 and ShHTL7 and PrKARRIKIN INSENSITIVE2d3 (PrKAI2d3) the putative orthologues in *Striga hermontica* and *Phelipanche ramosa,* respectively) (de Saint Germain *et al.,* 2016; de Saint Germain *et al.,* 2021; Yao *et al.,* 2016; Yao *et al.,* 2017; Yao *et al.,* 2018a, b).

As a further step, we evaluated whether CpD14 could complement the phenotypic defects of the *A. thaliana d14-1* mutant line. Three transgenic lines (#3.2, #7.5 and #9) were generated expressing the *CpD14* cDNA as a 6X-HA tagged fusion protein under the *A. thaliana D14* promoter (Supporting Information Fig. S7a). The shoot branching (Supporting Information Fig. S7 b,c) and plant height (Supporting Information Fig. S7 b,c) phenotypes of the *Atd14-1* mutant were not rescued by *CpD14* expression, as by contrast, was observed in the line transformed with the *AtD14* gene which was used as a positive control (Supporting Information Fig. S7 b,c). It is worth to note that, even if expressed under the same promoter, CpD14 was much less abundant in Arabidopsis leaves than AtD14 (Supporting Information Fig. S7a), suggesting a different stability or turnover of CpD14 compared to AtD14 or a lower expression due to lack of codon usage optimization between fungal coding and plant coding D14 homologues.

Although the complementation assay was not successful, the biochemical characterization of the protein clearly shows that CpD14 binds and hydrolyses GR24 natural stereoisomers thanks to the SDH catalytic triad.

In vitro* fungal development upon GR24 treatment is altered in strains defective of *CpD14

Three independent *C. parasitica* knock-out mutants (Δ*cpd14_48*, *Δcpd14_137*, Δ*cpd14_141)* were generated using site-directed double homologous recombination (Fig. 4a). Ninety-six hours post inoculation, the *in vitro* growth of the mutant strains under standard conditions was comparable to that of the WT strain (Fig. 4b,c). The same behaviour was shown by a control strain (D14_TC),

This article is protected by copyright. All rights reserved

which has been subjected to the process of genetic transformation but without the construct leading to the specific mutation on *CpD14* gene (Fig. 4b,c).

The effect of SLs on the mutant strains was then tested by considering an exposure to (+)-GR24. Notably, the *in vitro* growth of the three mutants was less inhibited compared to that of the WT or the control strain D14_TC (Fig. 4d). We also tested the effect of tolfenamic acid, which has been recently described as an inhibitor of plant SLs receptors (Hamiaux *et al.,* 2018). The tolfenamic acid treatment slightly reduced the *in vitro* fungal growth of wt and mutant strains but, notably, the treatment decreased the growth inhibition induced by GR24 in the wt strain (Fig. 5a), confirming its inhibitory activity towards GR24 perception also in fungi. Interestingly, the tolfenamic acid treatment did not influence the growth of Δ*cpd14* knock out mutants upon (+)-GR24 treatment (Fig. 5a) further confirming *in vivo* interaction between GR24 and CpD14.

To get further insights on the link between CpD14 and GR24 effect on fungal growth, we analysed the effect of zaxinone, another carotenoid-derived molecule which we previously described as a plant growth regulator also involved in the establishment of the AM symbiosis, as a rice line defective of the gene responsible for zaxinone synthesis showed a reduced mycorrhization (Wang *et al.,* 2019). We investigated the effect of zaxinone on wt and Δ*cpd14* mutant strains. Zaxinone exposure led to a strong growth inhibition of the wr strain and the same effect was observed in the Δ*cpd14* mutants (Fig. 5b), indicating that CpD14 is not involved in the response to another signalling apocarotenoid.

To investigate the putative involvement of CpD14 in the fungus-plant interaction, we performed a virulence assay. Wild type and Δ*cpd14* mutant strains were inoculated on chestnut cuttings and lesions were measured after 30 days. Under this condition, no difference was observed between wt and mutant strains (Supporting Information Fig. S8).

We also hypothesized that CpD14 could have an endogenous role; we thus investigated in *C. parasitica* the occurrence of genes putatively involved in carotenoid biosynthesis and cleavage, based on those described in the model fungus *Neurospora crassa.* We found genes encoding a putative cyclase and phytoene synthase (CpPHYSYN), a phytoene dehydrogenase (CpPHYDE), a carotenoid oxygenase (CpCARX), a neurosporaxanthin - torluene carotenoid oxygenase 2 (CpOCO) and an aldehyde dehydrogenase (CpADE). We then analysed their expression profile in the wt and the mutant strains. *CpPhySin* and *CpPhyADE*, which are placed at the beginning of the carotenoid pathway, showed a lower expression in both mutants compared to the wt strain while no difference was detected for *CpPHYDE*, *CpCARX* and *CpOCO* (Supporting Information Fig. S4

This article is protected by copyright. All rights reserved

b,c,d,e,f). This result indicates that the lack of CpD14 induces a perturbation on the expression of some genes of the carotenoid pathway and suggests that CpD14 could have also an endogenous role.

Discussion

In silico studies reveal putative homologues of D14 in fungi

SLs are multifunctional plant metabolites acting as a class of hormones controlling plant developmental processes and interactions with other organisms (Lopez-Raez *et al.,* 2017; Lanfranco *et al.,* 2018b; Carvalhais *et al.,* 2019); they were even shown to have an impact on human cell lines as anti-cancer, anti-inflammatory and anti-viral drugs (Prandi *et al.,* 2021). SLs have therefore multiple target organisms which, in turn, had to evolve a molecular machinery to perceive and respond to them. The SL receptor D14, with the unique feature of coupled enzyme and receptor functions, and several downstream signaling components have been characterized in plants (Mashiguchi *et al.,* 2021). So far, no SL receptor/early signaling components have been described in fungi. Unfortunately, AM fungi, which display the most studied biological response to SLs in the fungal kingdom, are not a suitable experimental system for a reverse genetic approach because of the lack of stable genetic transformation protocols. Here we exploited *C. parasitica,* a filamentous fungus, previously shown to be sensitive to (±)-GR24 (Belmondo *et al.,* 2016) and for which genetic and genomic resources are available (Crouch *et al.,* 2020), to look for candidate SLs receptors. Using the same biological assay set up by Belmondo *et al.* (2016), we demonstrated here that *C. parasitica* is more sensitive to GR24 isomers whose stereochemistry corresponds to natural SLs, pointing to a biological response strongly linked to specific SL stereochemistry.

A candidate protein, named CpD14, was identified by BlastP searches under low stringency conditions and characterized *in silico* using molecular homology modelling and docking. The 3D structure of CpD14, obtained using DAD2 as a template, showed the typical fold of α/β hydrolase enzymes; the alignment and superposition with petunia DAD2 and OsD14 revealed the conservation of the catalytic SDH triad. Docking simulations proved a good positioning of the ligand, correctly orienting the D-ring to the catalytic residues. These results, further confirmed by the correspondence between the docking pose of (+)-GR24 in CpD14 and its crystallographic pose in OsD14, support the prediction that CpD14 may interact with and hydrolyse SLs.

Our survey within fungal kingdom databases clearly shows the widespread occurrence in fungal

This article is protected by copyright. All rights reserved

genomes of putative homologues of CpD14 with a conserved SDH catalytic triad; this finding suggests their potential involvement in important adaptive functions. However, to our knowledge, none of these fungal genes, annotated as α/β hydrolases or hypothetical proteins, has been so far characterized through a reverse genetic approach. Phylogenetic reconstruction shows some degree of correlation with taxonomic groups. Notably, the sequences identified in genomes of AM fungi, as first hits using CpD14 as query, form a cluster of Glomeromycotina-only sequences (Fig. 2). It would be interesting to further characterize these sequences and test their involvement in SLs response.

CpD14 hydrolyses the natural stereoisomers of GR24 *in vitro* and is involved in the SLs-induced fungal growth suppression *in vivo*

In vitro biochemical characterization of the CpD14 recombinant protein, by using the tryptophan intrinsic fluorescence assay, demonstrated that it interacts with (+)-GR24 even if with a 20-fold lower affinity compared to RMS3/PsD14. Notably, CpD14 displays an α/β hydrolytic activity *in vitro* on GR24 with a preference for isomers showing natural stereochemistry, and this enzymatic activity requires an intact catalytic triad. In addition, we demonstrated that CpD14 forms a covalent complex with the D-ring *via* the histidine residue of the catalytic triad. This has been previously reported for plant SLs receptors such as RMS3/PsD14, AtD14, ShHTL7 and OsD14 (de Saint Germain *et al.,* 2016, Yao *et al.,* 2016; Yao *et al.,* 2017; Yao *et al.,* 2018). Thus, computational and *in vitro* biochemical analyses indicate that CpD14 is able to bind and hydrolyse SLs with a mechanism similar to the one deciphered for plant SL receptors.

To clarify the role of CpD14 in the suppression of fungal growth by GR24 observed *in vitro*, CpD14 knock-out mutants were generated by homologous recombination. The mutants displayed a reduced sensitivity to (+)-GR24 compared to the wt strain, although the response was not fully abolished. The lack of a complete insensitivity could be explained by the presence of a second gene in the *C. parasitica* genome encoding a protein with 49% identity to CpD14 that may partially complement lack of CpD14 function. The analysis of a double knock-out mutant can verify this hypothesis.

The exposure to tolfenamic acid, an inhibitor of plant SLs receptors (Hamiaux *et al.,* 2018), reduced the effect of GR24 on the growth of the wt *C. parasitica*, suggesting a conserved inhibitory activity on CpD14. Interestingly, tolfenamic acid did not exert any effect on the Δ*cpd14* mutants. The specificity of the response to SLs was assessed by considering zaxinone, a recently

This article is protected by copyright. All rights reserved

described natural metabolite which is also derived from the carotenoid pathway (Wang *et al.,* 2019). Zaxinone inhibited growth in the wt strain, similar to what observed for (+)-GR24; as well as in the Δ*cpd14* mutants. Thus, although the reasons of the inhibitory effect of zaxinone are unknown, these results clearly indicate that the response to zaxinone does not involve CpD14. Overall, these data demonstrate that *C. parasitica* growth reduction induced by (+)-GR24 is mediated by an active CpD14, a protein able to bind and hydrolyse (+)-GR24 *in vitro.* However, it must be noted here that CpD14 expression under the control of the *AtD14* promoter did not complement the *d14-1* mutation in *A. thaliana.* Beside protein abundance issues (Supporting Information Fig. S7a), we can also hypothesize that signalling components downstream of D14 may not be properly activated in the CpD14-complemented *A. thaliana* mutant. Indeed, by using the tryptophan intrinsic fluorescence assay, we could not verify the occurrence of CpD14 conformational changes upon SL binding, an event that is required for downstream signaling in plants (Yao *et al.,* 2018).

A still open question is the biological role of CpD14 in *C. parasitica*. The mutants do not display an obvious phenotype under standard laboratory growth conditions, unless they are exposed to bioactive stereoisomers of synthetic SLs. We hypothesized a theoretical interaction with plant-derived SLs in chestnut bark, the site of entry and initial pathogenic interaction in *C. parasitica*-chestnut. However, no differences were found between wt and mutant strains in a pathogenicity test performed on chestnut cuttings which allows to measure initial pathogenicity and virulence potential of the fungus. In contrast, in infections occurring in nature, a typical secondary symptom of *C. parasitica* infection are epicormic bud outgrowths around the canker region of the bark lesion, particularly in cankers with intensive lethal infection outcome (Rigling and Prospero 2018). In this regard, although no specific data are available for SLs presence and role in chestnut trees, we can speculate that such bud outgrowths may be linked to SLs regulation mediated by *C. parasitica* infection. Indeed, SLs were shown to be negative regulators of axillary bud outgrowth (Ruyter-Spira *et al.,* 2013), an activity that is maintained in the model tree poplar (Muhr *et al.,* 2016).

On the other hand, we can also speculate that *C. parasitica* uses CpD14 to hydrolyse endogenous carotenoid-derived molecules, which may be important for fungal metabolism (Avalos & Limón 2015). A survey of the *C. parasitica* genome allowed us to identify indeed several putative homologues of those genes involved in carotenoid and apocarotenoid metabolism, well described in the model fungus *Neurospora crassa*. Notably, these genes are expressed in the free-living

This article is protected by copyright. All rights reserved

mycelium of *C. parasitica,* and some were found to be de-regulated in the mutant strains. Comparing the metabolome and, notably, the apocarotenoids of WT with Δ*cpd14 C. parasitica*, may provide further insights on this intriguing possibility.

In conclusion, we have characterized a fungal gene encoding a member of the α/β hydrolase fold family of enzymes. *In silico* modelling, docking and *in vitro* assays demonstrated its ability to bind and hydrolyse natural GR24 stereoisomers. The characterization of knock-out fungal strains showed that the gene mediates fungal growth inhibition induced by SLs under controlled growth conditions. As a whole, our findings support the idea that SLs are multifunctional molecules acting in plant-microbe interactions. Their divergent roles in promoting root-symbiosis and influencing the growth of detrimental fungi may open new perspectives for agro-biotechnological applications.

Acknowledgements

This work was supported by baseline funding of the University of Turin (LL and VF) and the Competitive Research Grant (CRG2017) given to SA-B and LL from King Abdullah University of Science and Technology. We kindly acknowledge Molecular Discovery Ltd. for supporting GD'A, the Centro di Competenza sul Calcolo Scientifico (C3S) at the University of Turin (c3s.unito.it) for providing the computational time and resources, and BiKi Technologies for providing the BiKi LiFe Sciences suite. AdSG has received the support of the EU in the framework of the Marie-Curie FP7 COFUND People Programme, through the award of an AgreenSkills/AgreenSkills+ fellowship. The IJPB benefits from the support of Saclay Plant Sciences-SPS (ANR-17-EUR-0007). This work has benefited from the support of IJPB's Plant Observatory technological platforms and from the facilities and expertise of the I2BC proteomic platform (Proteomic-Gif, SICaPS) supported by Infrastructures en Biologie Santé et Agronomie, Ile de France Region, Plan Cancer, CNRS, and Paris-Sud University. The CHARM3AT Labex program (ANR-11-LABX-39) is also acknowledged for its support. VF has received a short-term mobility COST fellowship (COST Action FA 1206). We also thank William Conrad Ledford for assistance with the English language.

Author contributions: LL, VF and MT designed the investigation. VF and MF conducted experiments on growth assays and mutant generation and analyses; AdSG, DC, PLB and F-DB were involved in the biochemical assays and Arabidopsis complementation and GD'A and FS performed modelling and docking analyses. LL, MT, F-DB, FS, CP, FC and SA-B contributed to

This article is protected by copyright. All rights reserved

Accepted Article

results discussion and wrote the manuscript. VF, MF and AdSG contributed equally to this work.

Data availability

The data that support the findings of this study are available from the corresponding author upon reasonable request.

Accepted Article

This article is protected by copyright. All rights reserved

Accepted Article

References

Akiyama K, Matsuzaki K, Hayashi H. 2005. Plant sesquiterpenes induce hyphal branching in arbuscular mycorrhizal fungi. *Nature* **435**: 824-827.

Al-Babili S, Bouwmeester HJ. 2015. Strigolactones, a novel carotenoid-derived plant hormone. *Annual Review of Plant Biology* **66**: 161-186.

Allen TD, Dawe AL, Nuss DL, 2003. Use of cDNA microarrays to monitor transcriptional responses of the chestnut blight fungus *Cryphonectria parasitica* to infection by virulence-attenuating hypoviruses. *Eukaryotic Cell* **2**: 1253-1265.

Avalos J, Limón MC. 2015. Biological roles of fungal carotenoids. *Current Genetics* **61**: 309-324.

Belmondo S, Marschall R, Tudzynski P, López Ráez JA, Artuso E, Prandi C, Lanfranco L. 2017. Identification of genes involved in fungal responses to strigolactones using mutants from fungal pathogens. *Current Genetics* **63**: 201-213.

Besserer A, Bécard G, Jauneau A, Roux C, Séjalon-Delmas N. 2008. GR24, a synthetic analog of strigolactones, stimulates the mitosis and growth of the arbuscular mycorrhizal fungus *Gigaspora rosea* by boosting its energy metabolism. *Plant Physiology* **148**: 402-413.

Besserer A, Puech-Pagès V, Kiefer P, Gomez-Roldan V, Jauneau A, Roy S, Portais JC, Roux C, Bécard G, Séjalon-Delmas N. et al. 2006. Strigolactones stimulate arbuscular mycorrhizal fungi by activating mitochondria. *PLoS Biology* **4**: 1239-1247.

Bürger M, Chory J. 2020. The many models of strigolactone signaling. 2020. *Trends in Plant Science* **25**: 395-405.

Carroll AM, Sweigard JA, Valent B. 1994. Improved vectors for selecting resistance to hygromycin. *Fungal Genetics Newsletter* **41**: 22, 1-2.

Carvalhais LC, Rincon-Floreza VA, Brewer PB, Beveridge CA, Dennis PG, Schenk PM 2019. The ability of plants to produce strigolactones affects rhizosphere community composition of fungi but not bacteria. *Rhizosphere* **9**: 18-26.

Chevalier F, Nieminen K, Sánchez-Ferrero JC, Rodríguez ML, Chagoyen M, Hardtke CS, Cubas P. 2014. Strigolactone promotes degradation of DWARF14, anα/βhydrolase essential for strigolactone signaling in Arabidopsis. *The Plant Cell* **26**: 1134-1150.

Choi GH, Nuss DL, 1992. Hypovirulence of chestnut blight fungus conferred by an infectious viral cDNA. *Science* **257**: 800-803.

Churchill ACL, Ciuffetti LM, Hansen DR, Vanetten HD, Vanalfen N. 1990. Transformation of the fungal pathogen *Cryphonectria parasitica* with a variety of heterologous plasmids. *Current*

This article is protected by copyright. All rights reserved

Genetics **17**: 25-31.

Clough SJ, Bent AF. 1998. Floral dip: a simplified method for Agrobacterium-mediated transformation of Arabidopsis thaliana. *The Plant Journal* **16**: 735-743

Cook CE, Whichard LP, Turner B, Wall ME, Egley GH. 1966. Germination of witchweed (*Striga lutea* Lour.): isolation and properties of a potent stimulant. *Science* **154**: 1189-1190.

Crouch JA, Dawe A, Aerts A, Barry K, Churchill ACL, Grimwood J, Hillman BI, Milgroom MG, Pangilinan J, Smith M, *et al* . 2020. Genome sequence of the chestnut blight fungus *Cryphonectria parasitica* EP155: a fundamental resource for an archetypical invasive plant pathogen. *Phytopathology*; **110**: 1180-1188.

Dawe AL, Van Voorhies WA, Lau TA, Ulanov AV, Li Z. 2009. Major impacts on the primary metabolism of the plant pathogen *Cryphonectria parasitica* by the virulence-attenuating virus CHV1-EP713. *Microbiology* **155**: 3913-3921.

De Cuyper C, Fromentin J, Yocgo RE, De Keyser A, Guillotin B, Kunert K, Boyer FD, Goormachtig S. 2015. From lateral root density to nodule number, the strigolactone analogue GR24 shapes the root architecture of *Medicago truncatula*. *Journal of Experimental Botany* **66**: 137-146.

de Saint Germain A, Clavé G, Badet-Denisot MA, Pillot JP, Cornu D, Le Caer JP, Burger M, Pelissier F, Retailleau P, Turnbull C, *et al*. 2016. An histidine covalent receptor and butenolide complex mediates strigolactone perception. *Nature Chemical Biology* **12**: 787-794.

de Saint Germain A, Clavé G. Boyer FD. Synthesis of profluorescent strigolactone probes for biochemical studies. In: Cristina Prandi, Francesca Cardinale (eds) Strigolactones: Methods and Protocols (Springer US, 2021), Hatfield, Hertfordshire, UK pp 219-231.

Decherchi S, Bottegoni G, Spitaleri A, Rocchia W, Cavalli A. 2018. BiKi Life Sciences: a new suite for molecular dynamics and related methods in drug discovery. *Journal of Chemical Information and Modeling* **58**: 219-224.

Dor E, Joel DM, Kapulnik Y, Koltai H, Hershenhorn J. 2011. The synthetic strigolactone GR24 influences the growth pattern of phytopathogenic fungi. *Planta* **234**: 419-427.

Eusebio-Cope A, Sun LY, Tanaka T, Chiba S, Kasahara S, Suzuki N. 2015. The chestnut blight fungus for studies on virus/host and virus/virus interactions: From a natural to a model host. *Virology* **477**: 164-175.

Fiorilli V, Novero M, Lanfranco L. Evaluation of the effect of strigolactones and synthetic analogs on fungi. In: Cristina Prandi, Francesca Cardinale (eds). Strigolactones: Methods and Protocols

This article is protected by copyright. All rights reserved

(Springer US, 2021) Hatfield, Hertfordshire, UK,pp 75-89.

Foo E, Ferguson BJ, Reid JB. 2014. The potential roles of strigolactones and brassinosteroids in the autoregulation of nodulation pathway. *Annals Botany* **113**: 1037-1045.

Genre A, Chabaud M, Balzergue C, Puech-Pagès V, Novero M, Rey T, Fournier J, Rochange S, Bécard G, Bonfante P, *et al.* 2013. Short-chain chitin oligomers from arbuscular mycorrhizal fungi trigger nuclear Ca^{2+} spiking in *Medicago truncatula* roots and their production is enhanced by strigolactone. *The New Phytologist* **198**: 190–202.

Gomez-Roldan V, Fermas S, Brewer PB, Puech-Pagès V, Dun EA, Pillot JP, Letisse F, Matusova R, Danoun S, Portais JC, *et al.* 2008. Strigolactone inhibition of shoot branching. *Nature* **455**: 189-194.

Ha CV, Leyva-González MA, Osakabe Y, Tran UT, Nishiyama R, Watanabe Y, Tanaka M, Seki M, Yamaguchi S, Dong NV, *et al.* 2014. Positive regulatory role of strigolactone in plant responses to drought and salt stress. *Proceedings of the National Academy of Sciences of the United States of America* **111**: 851–856.

Hamiaux C, Drummond RS, Janssen BJ, Ledger SE, Cooney JM, Newcomb RD, Snowden KC. 2012. DAD2 is an α/β hydrolase likely to be involved in the perception of the plant branching hormone, strigolactone. *Current Biology* **22**: 2032-2036.

Hamiaux C, Drummond RSM, Luo Z, Lee HW, Sharma P, Janssen BJ, Perry NB, Denny WA, Snowden KC. 2018. Inhibition of strigolactone receptors by *N*-phenylanthranilic acid derivatives: structural and functional insights. *The Journal of Biological Chemistry* **293**: 6530-6543.

Hornak V, Abel R, Ojur A, Strockbine B, Roitberg A, Simmerling C. 2006. Comparison of multiple Amber force fields and development of improved protein backbone parameters. *Proteins*; **65**: 712-725.

Jorgensen WL, Chandrasekhar J, Madura JD. 1983. Comparison of simple potential functions for simulating liquid water. *Journal of Chemical Physics* **79**: 926.

Kamel L, Tang N, Malbreil M, San Clemente H, Le Marquer M, Roux C, Frei Dit Frey N. 2017. The comparison of expressed candidate secreted proteins from two arbuscular mycorrhizal fungi unravels common and specific molecular tools to invade different host plants. *Frontiers in Plant Science* **8**: 124.

Karimi, M., Bleys, A., Vanderhaeghen, R., Hilson, P. 2007. Building blocks for plant gene assembly. *Plant Physiology* **145**: 1183-1191.

Koltai H, C. Prandi C. (eds.), Strigolactones - Biology and Applications. Springer Nature 2019.

This article is protected by copyright. All rights reserved

Switzerland AG.

Lan X, Yao Z, Zhou Y, Shang J, Lin H, Nuss DL, Chen B. 2008. Deletion of the cpku80 gene in the chestnut blight fungus, *Cryphonectria parasitica*, enhances gene disruption efficiency. *Current Genetics* **53**: 59-66.

Lanfranco L, Fiorilli V, Gutjahr C. 2018. Partner communication and role of nutrients in the arbuscular mycorrhizal symbiosis. *The New Phytologist* **220**: 1031-1046.

Lanfranco L, Fiorilli V, Venice F, Bonfante P. 2018. Strigolactones cross the kingdoms: plants, fungi, and bacteria in the arbuscular mycorrhizal symbiosis. *Journal of Experimental Botany* **69**: 2175-2188.

Lin K, Limpens E, Zhang Z, Ivanov S, Saunders DG, Mu D, Pang E, Cao H, Cha H, Lin T, *et al.* 2014. Single nucleus genome sequencing reveals high similarity among nuclei of an endomycorrhizal fungus. *PLoS Genetics* **10**: e1004078.

Lombardi C, Artuso E, Grandi E, Lolli M, Spyrakis F, Priola E, Prandi C. 2017. Recent advances in the synthesis of analogues of phytohormones strigolactones with ring-closing metathesis as a key step. *Organic & Biomolecular Chemistry* **15**: 8218-8231.

Lopez-Obando M, Ligerot Y, Bonhomme S, Boyer F-D, Rameau C. 2015. Strigolactone biosynthesis and signaling in plant development. *Development* **142**: 3615-3619.

López-Ráez JA, Shirasu K, Foo E. 2017. Strigolactones in plant interactions with beneficial and detrimental organisms: the yin and yang. *Trends in Plant Science* **22**: 527-537.

Lovat CA, Donnelly DJ. 2019. Mechanisms and metabolomics of the host-pathogen interactions between chestnut (*Castanea* species) and chestnut blight (*Cryphonectria parasitica*). *Forest Pathology* **49**: e12562.

MacLean AM, Bravo A, Harrison MJ. 2017. Plant signalling and metabolic pathways enabling arbuscular mycorrhizal symbiosis. *The Plant Cell* **29**: 2319–2335.

Mashiguchi K, Seto Y, Yamaguchi S. 2021. Strigolactone biosynthesis, transport and perception. *The Plant Journal* **105**: 335-350.

McAdam EL, Hugill C, Fort S, Samain E, Cottaz S, Davies NW, Reid JB, Foo E. 2017. Determining the site of action of strigolactones during nodulation. *Plant Physiology* **175**: 529-542.

Muhr M, Prüfer N, Paulat M, Teichmann T. 2016. Knockdown of strigolactone biosynthesis genes in Populus affects BRANCHED1 expression and shoot architecture. *New Phytologist* **212:** 613-626.

Peláez-Vico MA, Bernabéu-Roda L, Kohlen W, Soto MJ, López-Ráez JA. 2016. Strigolactones in

This article is protected by copyright. All rights reserved

the rhizobium-legume symbiosis: stimulatory effect on bacterial surface motility and down-regulation of their levels in nodulated plants. *Plant Science* **245**: 119-127.

Prandi C, Kapulnik Y, Koltai H. 2021. Strigolactones: phytohormones with promising biomedical applications. *European Journal of Organic Chemistry* **29:** 4019-4026.

Pronk S, Pàll A, Schulz R, Larsson P, Bjelkmar P, Apostolov R, Shirts MR, Smith JC. 2013. GROMACS 4.5: A high-throughput and highly parallel open source molecular simulation toolkit. *Bioinformatics* **29**: 845-854.

Rigling, D, Prospero S. 2018. *Cryphonectria parasitica*, the causal agent of chestnut blight: invasion history, population biology and disease control. *Molecular Plant Pathology* **19:** 7-20.

Rochange S, Goormachtig S, Lopez-Raez JA, Gutjahr C. The role of strigolactones in plant-microbe interactions. In: Koltai H., Prandi C. (eds) Strigolactones - Biology and Applications. (Springer,. 2019) Switzerland AG. pp.121-142

Rostagno L, Prodi A, Turina M. 2010. Cpkk1, MAPKK of *Cryphonectria parasitica*, is necessary for virulence on chestnut. *Phytopathology* **10**: 1100-1110.

Ruyter-Spira C, Al-Babili S, van der Krol S, Bouwmeester H. 2013. The biology of strigolactones. *Trends in Plant Science* **18:** 72-83.

Salvioli A, Ghignone S, Novero M, Navazio L, Venice F, Bagnaresi P, Bonfante P. 2016. Symbiosis with an endobacterium increases the fitness of a mycorrhizal fungus, raising its bioenergetic potential. *The ISME Journal* **10**: 130-144.

Sanchez E, Artuso E, Lombardi C, Visentin I, Lace B, Saeed W, Lolli ML, Kobauri P, Ali Z, Spyrakis F, *et al.* 2018. Structure–activity relationships of strigolactones via a novel, quantitative *in planta* bioassay. *Journal of Experimental Botany* **69**: 2333-2343.

Schlemper TR, Leite MFA, Lucheta AR, Shimels M, Bouwmeester HJ, van Veen JA, Kuramae EE. 2017. Rhizobacterial community structure differences among sorghum cultivars in different growth stages and soils. *FEMS Microbiological Ecology* **93**: 8, 1-11.

Seto Y, Yasui R, Kameoka H, Tamiru M, Cao M, Terauchi R, Sakurada A, Hirano R, Kisugi T, Hanada A, *et al.* 2019. Strigolactone perception and deactivation by a hydrolase receptor DWARF14. *Nature Communication* **10**: 191, 1-10.

Shabek N, Ticchiarelli F, Mao H, Hinds TR, Leyser O, Zheng N. 2018. Structural plasticity of D3-D14 ubiquitin ligase in strigolactone signalling. *Nature* **563**: 652-656.

Spyrakis F, Benedetti P, Decherchi S, Rocchia W, Cavalli A, Alcaro S, Ortuso F, Baroni M, Cruciani G. 2015. A pipeline to enhance ligand virtual screening: integrating molecular dynamics

This article is protected by copyright. All rights reserved

and fingerprints for ligand and proteins. *The Journal of Chemical Information and Modeling* **55**: 2256-2274.

Tisserant E, Malbreil M, Kuo A, Kohler A, Symeonidi A, Balestrini R, Charron P, Duensing N, Frei dit Frey N, Gianinazzi-Pearson V, *et al.* 2013. Genome of an arbuscular mycorrhizal fungus provides insight into the oldest plant symbiosis. *Proceedings of the National Academy of Sciences of the United States of America* **110**: 20117-20122.

Toh S, Holbrook-Smith D, Stokes ME, Tsuchiya Y, McCourt P. 2014. Detection of parasitic plant suicide germination compounds using a high-throughput Arabidopsis HTL/KAI2 strigolactone perception system. *Chemistry and Biology* **21**: 988-998.

Tsuzuki S, Handa Y, Takeda N, Kawaguchi M. 2016. Strigolactone-induced putative secreted protein 1 is required for the establishment of symbiosis by the arbuscular mycorrhizal fungus *Rhizophagus irregularis*. *Molecular Plant Microbe Interactions* **29**: 277-286.

Umehara M, Hanada A, Yoshida S, Akiyama K, Arite T, Takeda-Kamiya N, Magome H, Kamiya Y, Shirasu K, Yoneyama K, *et al.* 2008. Inhibition of shoot branching by new terpenoid plant hormones. *Nature* **455**: 195–200.

Volpe V, Carotenuto G, Berzero C, Cagnina L, Puech-Pagès V, Genre A. 2020. Short chain chito-oligosaccharides promote arbuscular mycorrhizal colonization in *Medicago truncatula*. *Carbohydrate Polymers* **229**: 115505, 1-10.

Wang JY, Haider I, Jamil M, Fiorilli V, Saito Y, Mi J, Baz L, Kountche BA, Jia KP, Guo X, *et al.* 2019. The apocarotenoid metabolite zaxinone regulates growth and strigolactone biosynthesis in rice. *Nature Communication* 10: 810, 1-9.

Wang J, Lu L, Yang Y, Chen Q, Chen B. 2014. Proteomic analysis of *Cryphonectria parasitica* infected by a virulence-attenuating hypovirus. *Acta Microbiologica Sinica* **54**: 803-812.

Waterhouse A, Bertoni M, Bienert S, Studer G, Tauriello G, Gumienny R, Heer FT, de Beer TAP, Rempfer C, Bordoli L, *et al*. T. 2018. SWISS-MODEL: homology modelling of protein structures and complexes. *Nucleic Acids Research* **46**: W296-W303.

Waters MT, Gutjahr C, Bennett T, Nelson DC. 2017. Strigolactone signaling and evolution. *Annual Review of Plant Biology* **68**: 291-322.

Yao R, Chen L, Xie D. 2018a. Irreversible strigolactone recognition: a non-canonical mechanism for hormone perception. *Current Opinion in Plant Biology* **45**: 155-161.

Yao R, Ming Z, Yan L, Li S, Wang F, Ma S, Yu C, Yang M, Chen L, Chen L, *et al.* 2016. DWARF14 is a non-canonical hormone receptor for strigolactone. *Nature* **536**: 469-473.

This article is protected by copyright. All rights reserved

Yao R, Wang F, Ming Z, Du X, Chen L, Wang Y, Zhang W, Deng H, Xie D . 2017. ShHTL7 is a non-canonical receptor for strigolactones in root parasitic weeds. *Cell Research* **27**: 838-841.

Yao R, Wang L, Li Y, Chen L, Li S, Du X, Wang B, Yan J, Li J, Xie D. 2018. Rice DWARF14 acts as an unconventional hormone receptor for strigolactone. *Journal of Experimental Botany* **69**: 2355-2365.

Yoneyama K, Akiyama K, Brewer PB, Mori N, Kawano-Kawada M, Haruta S, Nishiwaki H, Yamauchi S, Xie X, Umehara M, *et al.* 2020. Hydroxyl carlactone derivatives are predominant strigolactones in *Arabidopsis*. *Plant Direct* **4**: e00219.

Zhao LH, Zhou XE, Yi W, Wu Z, Liu Y, Kang Y, Hou L, de Waal PW, Li S, Jiang Y, *et al.* 2015. Destabilization of strigolactone receptor DWARF14 by binding of ligand and E3-ligase signaling effector DWARF3. *Cell Research* **25:** 1219-1236.

Accepted Article

This article is protected by copyright. All rights reserved

Accepted Article

Figure legends

Figure 1. Molecular homology modelling and docking of CpD14. (a) Sequence alignment of DAD2, OsD14 and CpD14. The red boxes indicate the catalytic residues. **(b)** Homology model of CpD14 shown as light blue cartoon. The catalytic residues are shown as capped sticks and labelled. **(c)** Structural alignment of the CpD14 model and of the DAD2 template (Protein Data Bank code: 4ndp; light blue and light pink, respectively). Helices α1-α4 are labelled. The catalytic residues (Ser, Asp, His: SDH) are labelled and shown as capped sticks in the inset. **(d)** Docking pose of (+)-GR24 in the CpD14 model binding site. The compound and some of the residues defining the binding site are shown as capped sticks and labelled. Hydrogen bonds are represented as dashed lines.

Figure 2. Phylogenetic analysis of putative fungal D14 homologues. Through BLAST analysis, several fungal D14-like homologues conserving the SDH catalytic triad were retrieved from fungal genomes. Proteins obtained were aligned with Clustal Omega and the obtained alignments were used to build a phylogenetic tree using the ML method (using IqTree webserver with automatic substitution model selection). CpD14 is shown in bold with larger font size. Tree topology allows to identify clades hosting only protein belonging to Ascomycota, Basidiomycota, Mucoromycota and Glomeromycota, while other clades host proteins from fungi belonging to different taxonomical groups. For some fungi, two α/β hydrolases conserving the Ser/His/Asp catalytic triad could be found. The second blast hit in each genome (and less conserved compared to CpD14) is in red ink.

Figure 3. Biochemical characterization of CpD14. Biochemical analysis of the interaction between the RMS3/PsD14 and CpD14 proteins and GR24 isomers based on intrinsic tryptophan fluorescence **(a,b)**. Plots of fluorescence intensity *versus* strigolactones (SL) concentrations. The change in intrinsic fluorescence of RMS3 **(a)** and CpD14 **(b)** was monitored and used to determine the apparent K_D values. The plots represent the mean of two replicates and the experiments were repeated at least three times. Error bars represent the SD of three replicates (means ± SD, n = 3). The analysis was performed with GraphPad Prism 8.0 Software. CpD14 enzymatic activity towards GR24 isomers **(c)**. (+)-GR24, (–)-GR24, (+)-2'-*epi*-GR24 and (–)-2'-*epi*-GR24 at 10 µM were incubated with RMS3, CpD14 and CpD14^{S104} at 5 µM for 150 min at 25°C. UPLC-UV (260

This article is protected by copyright. All rights reserved

nm) was used to detect the remaining amount of GR24 isomers. Columns represent the mean value of the hydrolysis rate calculated from the remaining GR24 isomers, quantified in comparison with (±)-1-indanol, as internal standard. Error bars represent the SD of three replicates (means ± SD, n = 3). The asterisks indicate statistical significance from the CpD14 protein sample as ***, $p \leq 0.001$ as measured by Kruskal-Wallis test. Mass spectrometry characterization of covalent CpD14-ligand complexes. Deconvoluted electrospray mass spectra of CpD14 before **(d)** and after adding (+)-GR24 **(e)** or (–)-GR24 (f). Peaks with an asterisk correspond to proteins covalently bound to a ligand. The mass increments are measured for different protein-ligand complexes: 96.4 Da for (+)-GR24) and (–)-GR24). Deconvoluted electrospray mass spectra of $CpD14^{S104A}$ **(g)**. Fragmentation spectra of unmodified **(h)** and ligand-modified peptide **(i)**. Labeled peaks correspond to b and y fragments of the double charged precursor ion displayed on the top. The His residue (H281) modified by the ligand is underlined on the sequence. In red formula of the adduct determined by MS.

Figure 4. Characterization of the *CpD14* knock-out mutants. (a) Scheme of the knock-out construct. CpD14 knock-out mutants were obtained through double homologous recombination with a construct carrying a hygromycin B resistance cassette interrupting the gene sequence. Around 1kb upstream and downstream sequences of the *CpD14* gene were used to induce homologous recombination. Primers used for the screening of transformed colonies are shown. **(b, c)** Colony growth pattern of *C. parasitica* wild type (WT) and Δ*cpd14* mutants grown under normal condition. *C. parasitica* WT, Δ*cpd14* mutants (Δ*cpd14_48*; Δ*cpD14_141*; Δ*cpD14_137*) and negative transformation control (D14_TC) strains were grown on B5 solid medium + 2% glucose at 2025°C in the dark. Histograms represent the colony growth diameter of each strain after 48, 72 and 96 h of inoculation. Each strain was analyzed in triplicate. Data for each condition are presented as mean ± SE. nsd: no statistically significant difference. **(c)** Pictures taken with a stereomicroscope at the edge of the colony, 96 h post-inoculation. Bars 100 μm. **(d)** Effect of (+)-GR24 on the growth of *C. parasitica* WT and Δ*cpd14* mutants. *C. parasitica* WT, Δ*cpd14* mutants (Δ*cpd14_48*; Δ*cpD14_141*; Δ*cpD14_137*) and negative transformation control (D14_TC) strains were grown on B5 solid medium (supplemented with 2% glucose) at 20 °C in the dark. Histograms represent the decreased growth (%) of each strain obtained comparing strain colony diameter upon (+)-GR24 treatment with that measured upon mock treatment (acetone) 48, 72 and

This article is protected by copyright. All rights reserved

96 h after inoculation. Each strain was analysed in triplicate. Data for each condition are presented as mean ± SE. Different letters indicate statistically significant difference ($p< 0.05$, ANOVA) within each time point.

Figure 5. Effect of tolfenamic acid (TA) and zaxinone treatments on *C. parasitica* wild type (WT) **and Δ*cpd14* mutants. (a)** *C. parasitica* WT and Δ*cpd14* mutants (Δ*cpd14_48*; Δ*cpD14_141*; Δ*cpD14_137*) strains were grown on B5 solid medium (supplemented with 2% glucose) at 20°C in the dark. Histograms represent the decreased growth (%) of each strain obtained comparing colony diameter upon (+)-GR24, tolfenamic acid (T.A, a strigolactones (SL) receptor inhibitor (Hamiaux *et al*., 2018) and tolfenamic acid + (+)-GR24 treatments with the colony diameter measured upon the corresponding mock treatment (acetone, DMSO, DMSO + acetone, respectively) 48, 72 and 96 h after inoculation. Each molecule was added once in the media: (+)-GR24 had a final concentration of 10^{-4} M while tolfenamic acid had a final concentration of 10^{-6} M. **(b)** Effect of zaxinone treatments on *C. parasitica* WT and Δ*cpd14* mutants. *C. parasitica* WT, Δ*cpd14* mutants (Δ*cpd14_48*; Δ*cpD14_141*; Δ*cpD14_137*) and negative transformation control (D14_TC) strains were grown on B5 solid medium (supplemented with 2% glucose) at 20 °C in the dark. Histograms represent the decreased growth (%) of each strains obtained comparing colony diameter upon zaxinone (Wang *et al.,* 2019) treatment with that measured upon mock treatment (acetone) 48, 72 and 96 h after inoculation. Each strain was analysed in triplicate. Data for each condition are presented as mean ± SE. Different letters indicate statistically significant differences ($p< 0.05$, ANOVA) within each time point. nsd: no statistically significant difference.

Supporting information

Figure S1. Effect of the four GR24 stereoisomers on *Cryphonectria parasitica* growth.

Figure S2. Ramachandran plot of the CpD14 model.

Figure S3. Modelling and docking of CpD14 with DAD2 and OsD14.

Figure S4. Expression level of *CpD14* and genes putatively involved in carotenoid

This article is protected by copyright. All rights reserved

biosynthesis and cleavage in *Cryphonectria parasitica* mycelia.

Figure S5. Intrinsic tryptophan fluorescence of RMS3 and CpD14 proteins in the presence of SL analogues and thermostability analysed by nanoDSF.

Figure S6. Structures of SL profluorescent probes, and enzymatic kinetics for CpD14 (1 µM) and RMS3 (0.33 µM).

Figure S7. Complementation assay in *Arabidopsis thaliana atd14-1* mutant line.

Figure S8. *Cryphonectria parasitica* virulence assay on chestnut cuttings.

Table S1: List of primers.

Accepted Article

This article is protected by copyright. All rights reserved

Accepted Article

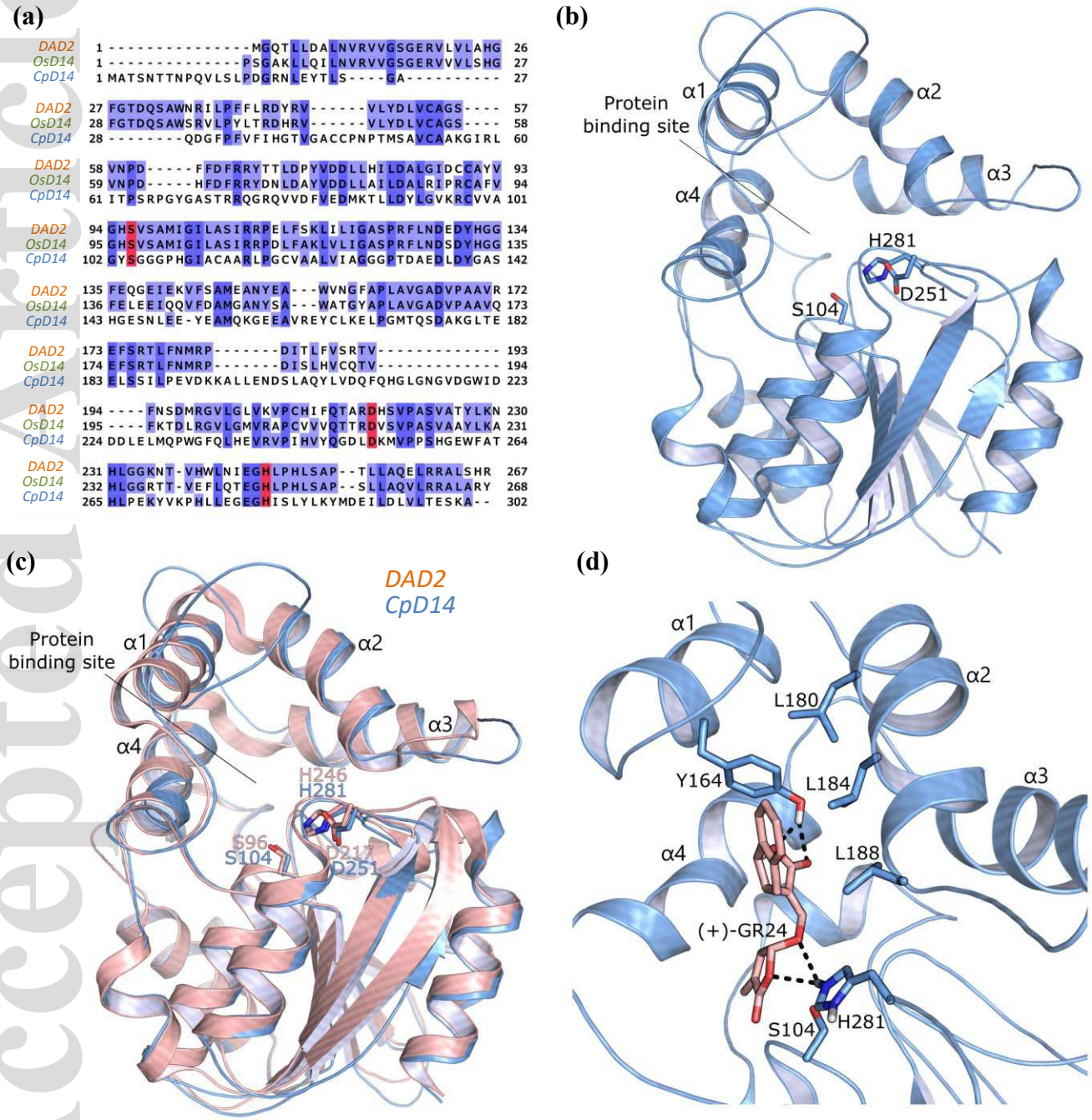

Figure 1

This article is protected by copyright. All rights reserved

Accepted Article

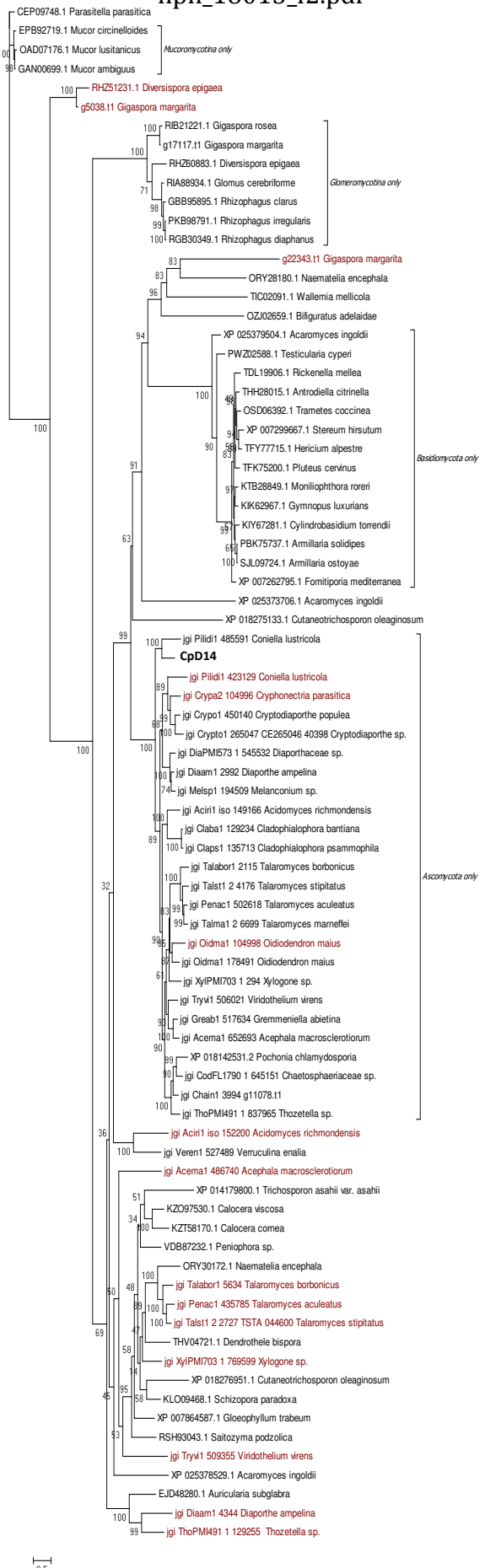

Figure 2

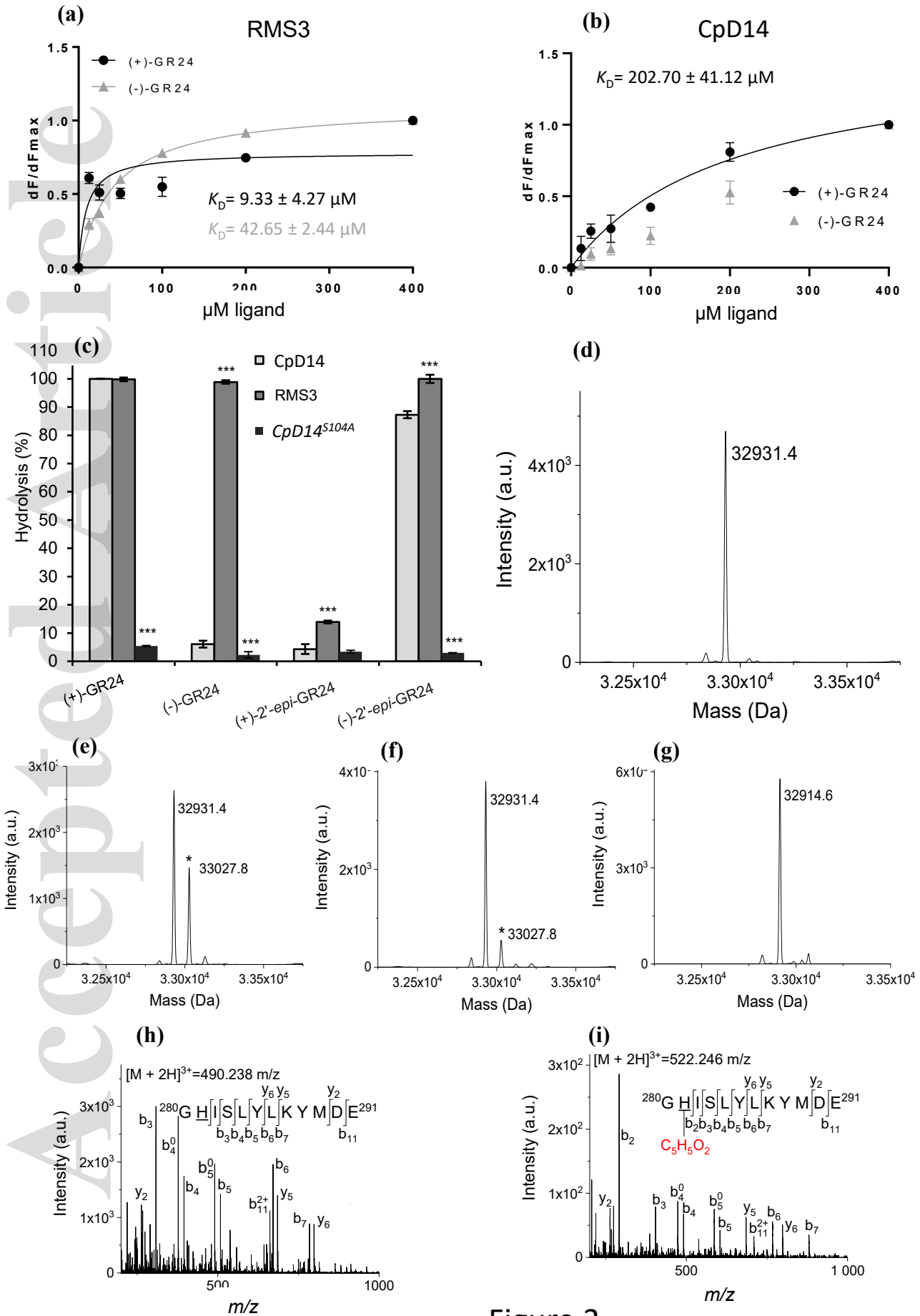

Figure 3

Accepted Article

Accepted Article

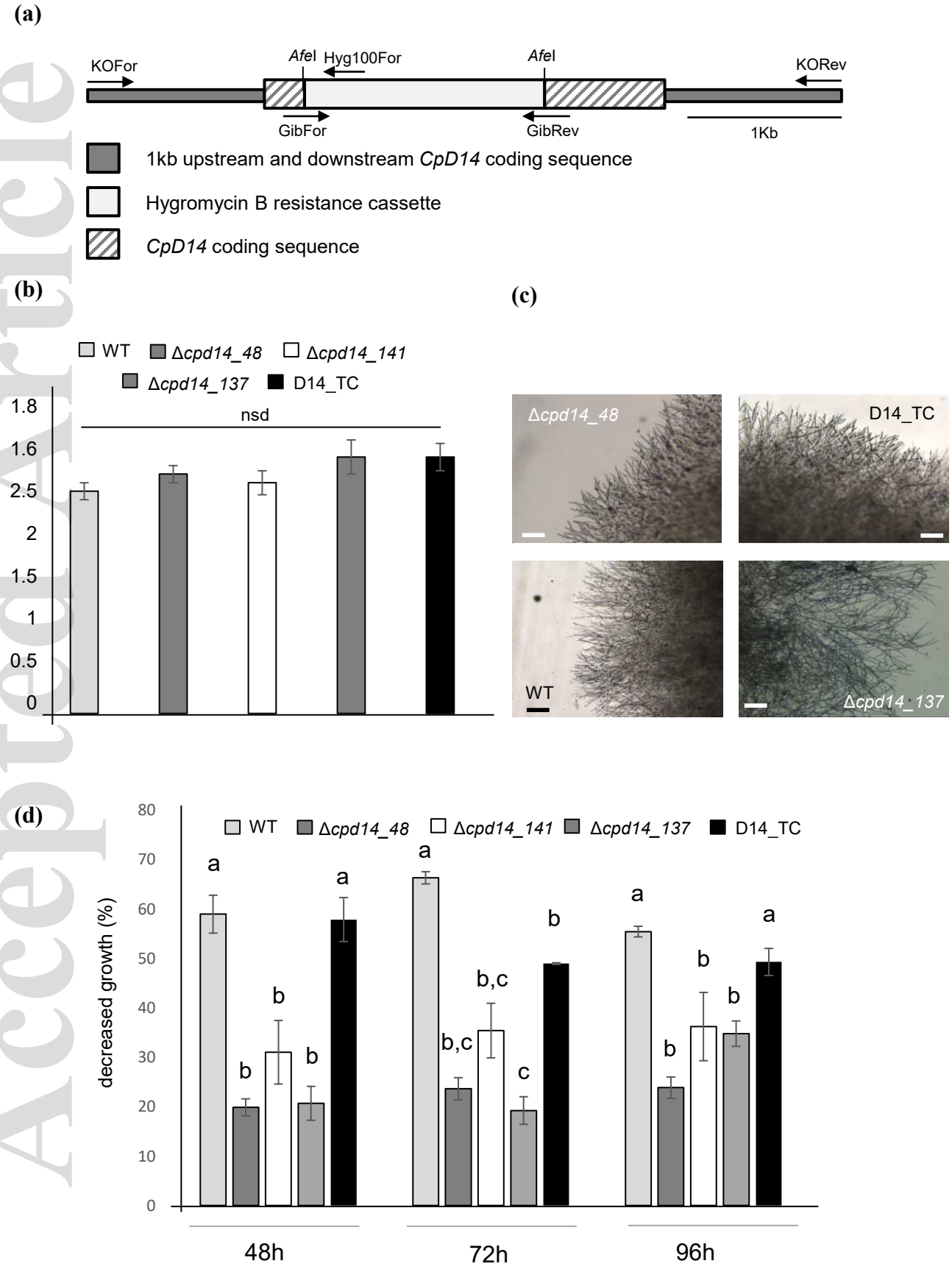

Figure 4

Accepted Article

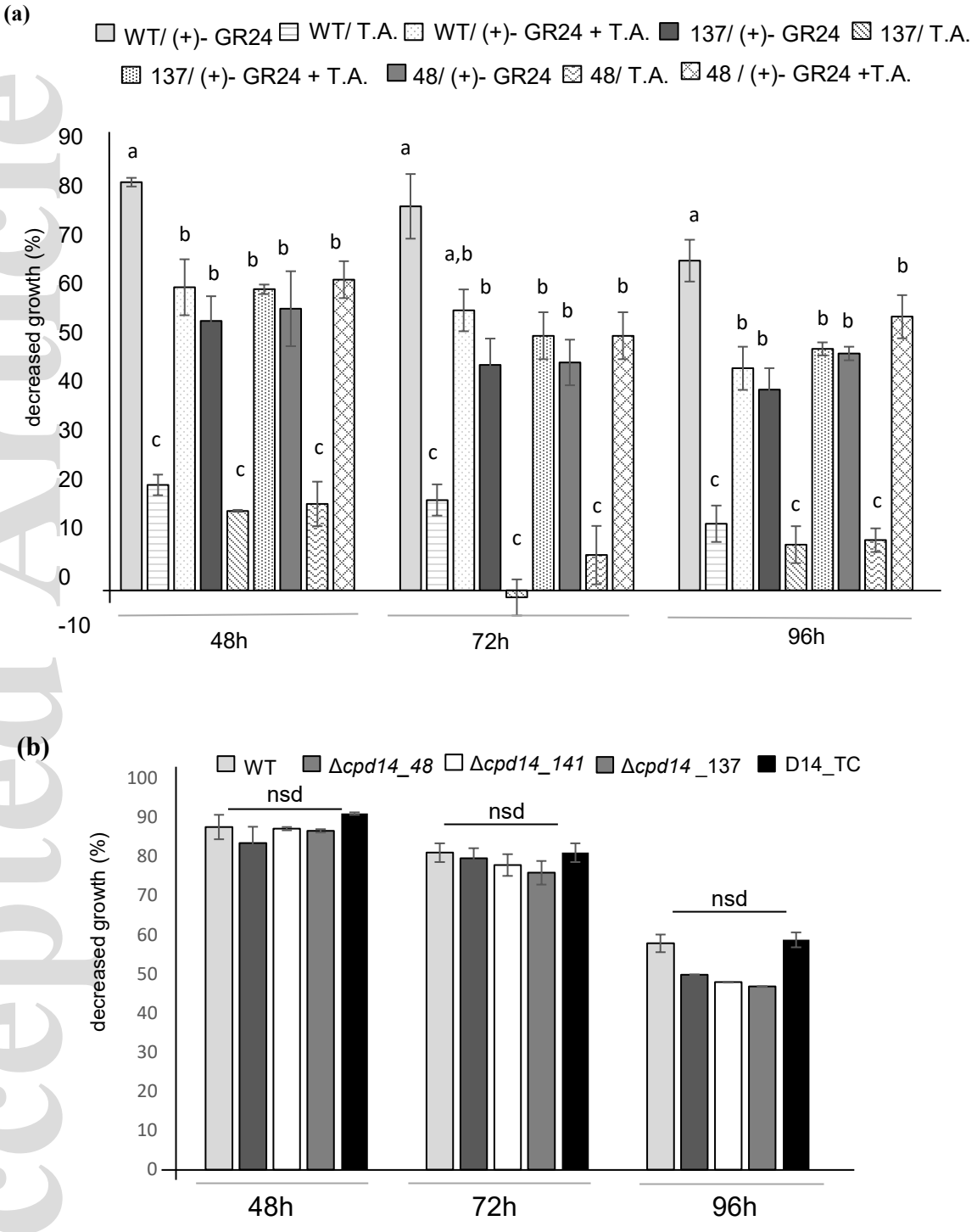

Figure 5

This article is protected by copyright. All rights reserved